

## Chapter 11

# RADIO OBSERVATIONS OF CORONAL MASS EJECTIONS

Angelos Vourlidas

*Solar Physics Branch, Naval Research Laboratory, Washington, DC*

vourlidas@nrl.navy.mil

**Abstract** In this chapter we review the status of CME observations in radio wavelengths with an emphasis on imaging. It is an area of renewed interest since 1996 due to the upgrade of the Nancay radioheliograph in conjunction with the continuous coverage of the solar corona from the EIT and LASCO instruments aboard *SOHO*. Also covered are analyses of Nobeyama Radioheliograph data and spectral data from a plethora of spectrographs around the world. We will point out the shortcomings of the current instrumentation and the ways that FASR could contribute. A summary of the current understanding of the physical processes that are involved in the radio emission from CMEs will be given.

**Keywords:** Sun: Corona, Sun: Coronal Mass Ejections, Sun:Radio

## 1. Coronal Mass Ejections

### 1.1 A Brief CME Primer

A Coronal Mass Ejection (CME) is, by definition, the expulsion of coronal plasma and magnetic field entrained therein into the heliosphere. The event is detected in white light by Thompson scattering of the photospheric light by the coronal electrons in the ejected mass. The first CME was discovered on December 14, 1971 by the *OSO-7* orbiting coronagraph (Tousey 1973) which recorded only a small number of events (Howard *et al.* 1975). *Skylab* observations quickly followed and allowed the first study of CME properties (Gosling *et al.* 1974). Observations from many thousands of events have been collected since, from a series of space-borne coronagraphs: *Solwind* (Michels *et al.* 1980), *SMM/CP* (MacQueen *et al.* 1980) and currently *SOHO/LASCO* (Brueckner *et al.* 1995). The average properties of CMEs are now well es-

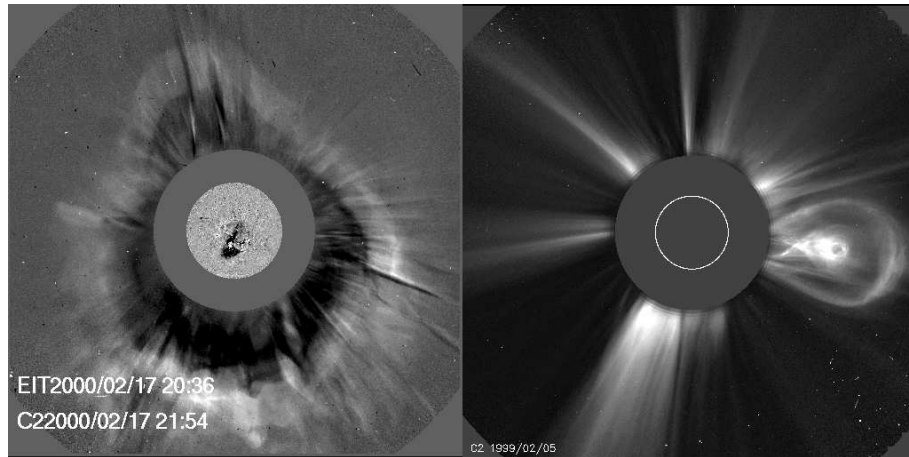


Figure 11.1. *Left panel:* Halo CME observed by LASCO/C2 on February 17, 2000. An EIT 195Å difference image is inserted to show the extent of the dimming in the low corona. Both images are differences between subsequent frames. *Right panel:* A typical 3-part CME along the western limb.

established (Hundhausen et al 1984; Howard *et al.* 1985; Hundhausen 1999; St Cyr *et al.* 1999; Vourlidas *et al.* 2002). Earth-directed CMEs, called “halo” CMEs because the ejected material surrounds the coronagraph occulter like a halo, were first recognized in *Solwind* images (Howard *et al.* 1982). The left panel of Figure 11.1 shows a typical example of a halo CME as observed by the LASCO/C2 coronagraph. Coronal ejections come in many shapes but one of the simplest forms (and hence usually refer to as “typical”) is the three part CME comprising a leading edge, followed by a dark cavity and a bright core (Fig 11.1, right panel).

In the years since their discovery, CMEs have come to be recognized as an important means of energy release in the solar corona and halo CMEs, in particular, as the major driver of the physical conditions in the Sun-Earth system (Webb *et al.* 2000; Webb *et al.* 2001; Plunkett *et al.* 2001). For an alternative view see (Cane, Richardson & StCyr 2000). In an average event,  $10^{14} - 10^{16}$  g of material is ejected into the heliosphere with speeds ranging from 100 to 2000 km/s (Howard *et al.* 1985; Hundhausen, Burkepile & StCyr 1994). CMEs might play an important role in the evolution of solar magnetism (Low 2001) since an amount of solar magnetic flux (not directly measured but potentially significant) is removed during the ejection process. Due to their large propagation speeds, CMEs can also drive interplanetary (IP) shocks (Cane 1984; Sheeley *et al.* 1985). IP shocks could be the sources of the accelerated particles (Reames 1999) that together with earth-directed CME mass and entrained magnetic field can severely affect geospace. Consequently, their study is very important for

understanding and ultimately predicting space weather conditions. For a more detailed review of CMEs refer to the articles in the *Coronal Mass Ejections* monograph (Crooker, Joselyn & Feynman 1997) and references therein.

CMEs are almost exclusively observed by white-light orbiting coronagraphs, which by design occult the solar disk. Thus, the initiation and early stages of the event are not visible and observations from other instruments, such as EUV imagers, must be employed. However, data analysis has been hampered by varying instrument cadences, fields of view, and telemetry restrictions. A thorough understanding of the CME phenomenon still eludes us. This is an area where radio astronomy can help. Radio telescopes can observe both the solar disk and the corona out to a few solar radii, at many frequencies and with high cadence ( $< 1$  s), while data acquisition issues are easily handled for ground-based instruments.

I begin with a short summary of the types of radio emissions that can be detected. In the next section, I review the work on radio CME observations since the launch of the *SOHO* satellite (Domingo, Fleck & Poland 1995). I conclude with a discussion of the issues confronting current radio CME observations and how they can be addressed by future instrumentation, such as the *Frequency Agile Solar Radiotelescope* (FASR) to bring radio observations to the forefront of CME science.

## 1.2 Radio Emissions Associated with CMEs

For the sake of the current discussion, we can divide radio emissions into two classes, thermal and non-thermal, based on the frequency dependence of the source radio flux density,  $S(\nu)$ , or, for spatially resolved measurements, the brightness temperature,  $T_b(\nu)$  (Gary & Hurford, Chapter 4). For optically-thin thermal sources,  $T_b(\nu) \propto \nu^{-2}$  while for optically-thin non-thermal ones,  $T_b(\nu) \propto \nu^{-\alpha}$ ,  $\alpha > 2$ . In the case of CMEs, there are possibly three relevant radio emission mechanisms; thermal free-free, non-thermal gyrosynchrotron and plasma emission. Here, I give only a very brief account of the relevant mechanisms as they pertain to CMEs. Complete discussion of the radio emission from the Sun can be found elsewhere (Dulk 1985).

**1.2.1 Thermal free-free.** The plasma entrained in the expanding magnetic field of the CME will produce optically thin free-free emission. The characteristics of this process are well understood and are described in detail in this volume (Gary & Hurford, Chapter 4; Gelfreikh, Chapter 6). The free-free emitting structures will look very similar to the structures seen by the white light coronagraphs since both correspond to multi-thermal plasmas and depend on the emission measure of the electrons; namely,  $\int n_e dl$  for Thompson scattering and  $\int n_e^2 dl$  for free-free, where  $n_e$  is the density of the coronal electrons. Besides the electron density, one may also derive the inhomogeneity

of the emitting structures from a detailed comparison between the two regimes. CMEs have coronal temperatures and low densities and hence their free-free emission is expected to be very optically thin and difficult to observe, especially in the presence of the much brighter emissions from non-thermal mechanisms (Figure 11.2).

**1.2.2 Nonthermal Gyrosynchrotron.** Gyrosynchrotron emission is routinely observed in flares (Bastian, Benz & Gary 1998) and could be present in CMEs since they are capable of accelerating electrons to high energies (Kahler *et al.* 1986). The gyrosynchrotron emission from even a small number of non-thermal electrons, entrained in the CME magnetic field, can easily exceed the thermal emission by a few orders of magnitude. Therefore, it is much easier to detect. Due to the dependence of gyrosynchrotron emission on the magnetic field, the brighter signal will correspond to the locations of the strongest magnetic field within the CME but the overall morphology will be similar to the white light CME. Gyroemission at low frequencies is suppressed in the presence of plasma where the index of refraction deviates from unity (Razin-Tsytovich suppression). This effect can be used as an additional diag-

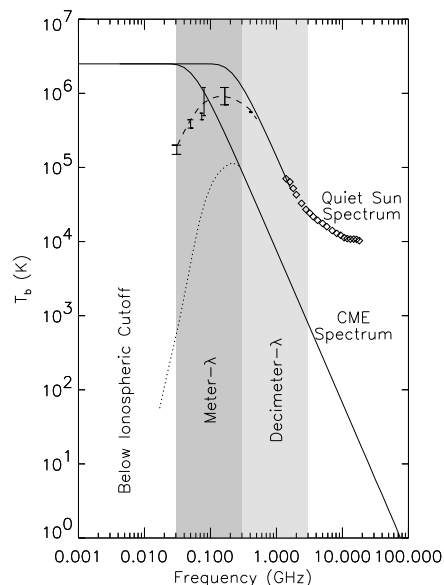


*Figure 11.2.* Simulated free-free radio spectra for the quiet Sun and a typical CME ( $n_e = 3.5 \times 10^7 \text{ cm}^{-3}$ ,  $T_e = 2.5 \text{ MK}$ ,  $L = 4.4 \times 10^{10} \text{ cm}$ ). The effects of refraction and reflection at the plasma layer are shown by the dashed and dotted lines, respectively. Diamonds are measurements by Zirin, Baumert & Hurdford 1991. The bars, below 1 GHz, represent the range of measurements at a few relevant frequencies from Lantos *et al.* 1980 and Wang, Schmahel & Kundu 1987. From Bastian & Gary 1997.

nostic of the density of the ambient (thermal) electrons and the magnetic field strength.

**1.2.3 Non-thermal Plasma Emissions.** Plasma emission is the most prevalent emission from CME structures and involves the efficient conversion of electron energy into a natural wave-mode of the plasma (e.g., trapped Langmuir waves) and the subsequent conversion to transverse waves that can escape to space as plasma radiation. This occurs at the plasma frequency and its second harmonic but rarely at higher harmonics. It is important mostly for frequencies below a few hundred MHz. Due to optical thickness effects, the plasma radiation is strongly reabsorbed at high frequencies (above 0.1–0.3 MHz for the fundamental and 2–5 GHz for the 2nd harmonic). It is the accepted emission mechanism for type II and IV-IVm solar bursts. Type-II bursts are associated with shocks driven by CME fronts and flares (Cane 1984; Gopalswamy *et al.* 1998a; Cliver, Webb & Howard 1999) while type-IV are stationary bursts that seem to be associated with the CME material following the leading edge. Moving type-IVs (IVm) are outward-moving radio blobs and are also associated with CMEs. They occur very rarely and are classified in three types: isolated plasmoids (Wagner *et al.* 1981), expanding arches and advancing fronts (Stewart 1985). It should be noted that plasma emission is not the only possible emission mechanism for IVms. An alternative explanation is gyrosynchrotron emission.

Imaging observations of such bursts at a single or few widely spaced frequencies are of rather limited use. First, the source morphology is entirely different from the white-light CME because plasma emission arises near the plasma level or its second harmonic, making it difficult to directly compare structures. Second, plasma radiation tends to be very bright and can easily mask the much weaker thermal free-free emission. Third, it is very difficult to derive information on the physical parameters of the emitting sources because of the complexity of the plasma emission processes. However, imaging over many closely spaced frequencies over the relevant frequency range, as FASR will do, will provide spatially resolved spectra over the entire emitting volume and may allow for more complete interpretation of such events.

## 2. Radio CME Observations during Cycle 23

The concept of ejection of coronal material has been around for a long time (Morrison 1954; Gold 1955) owing mainly to the early radio observations of moving type-IV (Boichot 1957) and type-II (Payne-Scott, Yabsley & Bolton 1947) bursts. However, the true extent of the CME phenomenon became apparent with the white light observations from orbiting coronagraphs in the last 30 years. Joint imaging radio and white light CME analyses have been rare because of the limited observing windows of both ground-based and earth-

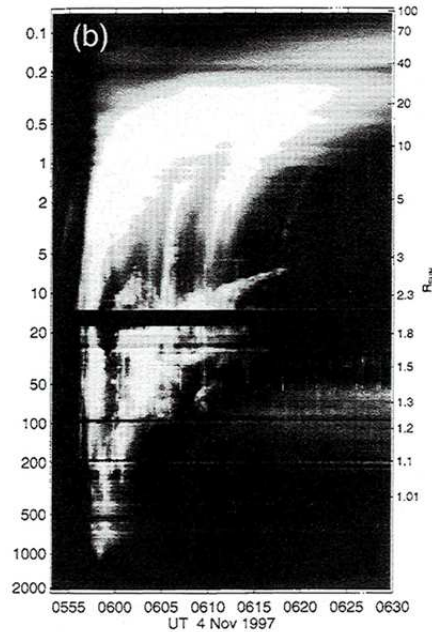


Figure 11.3. Example of a fairly complete spectral coverage of a CME event from 2 GHz to 100 kHz. The frequency axis on the left is in MHz units and the heliocentric distance axis on the right is in solar radii. From Dulk *et al.* 2000

orbiting instruments. Since 1996, this situation has greatly improved with the operation of the LASCO coronagraphs aboard the *SOHO* satellite which monitor the Sun continuously from the L1 point. Moreover, new and/or upgraded radio instruments have become operational in the last few years. They include solar imaging interferometers such as the Nobeyama Radioheliograph (NoRH; Nakajima *et al.* 1994) observing at 17 and 34 GHz, the upgraded Nanay Radioheliograph (NRH; Kerdraon & Delouis 1997) observing at up to 10 frequencies between 164–435 MHz, and the addition of 74 MHz capability at the Very Large Array (VLA). CME observations have also been reported from the Gauribidanour Radioheliograph (GRH; Ramesh *et al.* 1998) and Ooty (Manoharan *et al.* 2001). On the spectral front, there have been important advances in the study of IP bursts with the addition of space-based observations at frequencies below 14 MHz from the WAVES instrument (Bougeret *et al.* 1995) aboard the *WIND* satellite. Several ground-based spectrometers have also been upgraded (Potsdam, Odrejev, IZMIRAN) or constructed (BIRS, SRBL, Artemis, Oporto). We can now track the radio emission spectrum from the chromosphere (a few GHz) all the way to the Earth (a few kHz) (Figure 11.3).

Combined radio/EUV/LASCO observations have led to new insights on the physics of CMEs. For these reasons, this chapter is focused on the significant amount of radio work during the rising phase of solar cycle 23. The emphasis is on direct radio imaging of CME structures but work on what can be considered as indirect imaging (e.g., type-II sources, spectroscopic observations, etc.) is also discussed. We present the most important results in the following.

## 2.1 CME Detection

Direct CME detection in radio has great potential for important contributions to space weather studies because of the ability to track the event from its nascent stages on the disk to the outer corona. Despite the availability of better instrumentation there has been no detection of the thermal emission from CMEs so far. Gary *et al.* 1998 made the first science observations with the new 74 MHz VLA band looking specifically for CME thermal signatures. Two CMEs occurred during the observing period. Despite the radio data's excellent sensitivity (signal-to-noise ratio of 3000:1), no signatures of the CMEs were detected. Faint sources from several CME fronts were detected at NRH frequencies (Maia *et al.* 2000). Figure 11.4 is the best example. The sources moved at speeds comparable to the CME white light front and had brightness temperatures consistent with thermal sources (a few  $\times 10^4$  K). The polarization and spectral behavior, however, clearly showed that they were non-thermal sources. These results do not support the earlier detections of thermal CME emission (Gopalswamy & Kundu 1992; Sheridan *et al.* 1978) although those were made at very low frequencies ( $< 80$  MHz), which are not easily accessible with today's imaging instrumentation. The opening of the overlying streamer during the early stages of a CME was imaged by GRH at 109 MHz and an estimate of the mass at the leading edge was derived (Kathiravan, Ramesh & Subramanian 2002). Unfortunately, GRH lacks the capability to follow the event in time. It appears, therefore, that a radio instrument finely tuned to CME characteristics is needed. We will return to this point later.

## 2.2 CME Development

Thermal emission is not the only probe to the physics of CMEs. As we mentioned earlier, non-thermal emissions are easily detectable and their imaging can tell us a great deal about the development of the CME in the low corona.

The main advantages of coronal radio observations over other wavelengths are the high cadence ( $< 1$  s) and large field of view (active region to  $2\text{--}3 R_{\odot}$ , depending on observing wavelength). The first joint analysis of a CME with LASCO and the upgraded NRH (Maia *et al.* 1998; Pick *et al.* 1998) revealed multiple loop systems participating in the eruption process. The development of the eruption was shown more clearly in the imaging of the 1997 November



Figure 11.4. April 20, 1998 : Radio source progression seen by the NRH at 3 distinct frequencies. The sources is likely associated with the front of the white-light CME (Vourlidas *et al.* 1999).

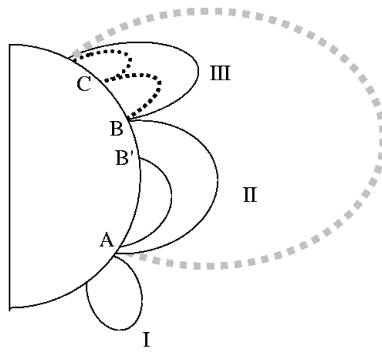


Figure 11.5. 1997 November 6: Schematic of the CME development as inferred from the NRH observations. From Maia *et al.* 1999.

6 event (Maia *et al.* 1999) where activated loop systems were traced from the flare site to the south of the equator to a active region behind the limb and north of the equator (Figure 11.5). Most importantly, most of the low-corona CME development took place within 4–5 min, much faster than the cadence of the LASCO or EIT instruments. In another large event, the radio sources spread through the solar disk in < 15 min (Maia *et al.* 2001). A similar analysis of a halo CME (Pohjolainen *et al.* 2001) verified the above conclusions. In addition, they showed that part of the ejected loops can be traced by their radio emission before their liftoff. The radio observations imaged a set of transequatorial loops that lifted as part of the CME, leaving an EUV dimming behind (Figure 11.6).

This result demonstrates the capability of radio imaging in tracing the source regions of the Earth-directed CME ejecta and consequently the possibility of estimating the mass and magnetic field in these ejecta, perhaps through the use of auxiliary observations (EUV, SXR). The radio observations also reveal the

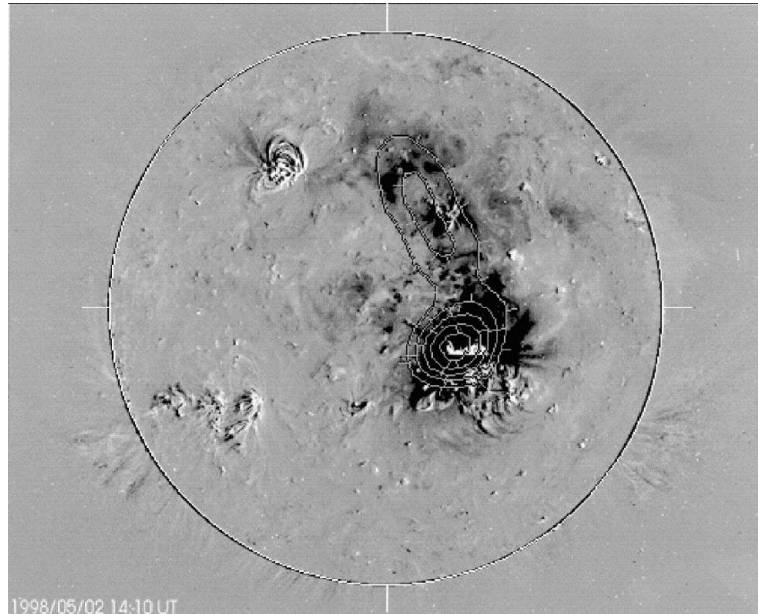


Figure 11.6. 195Å difference image on 1998 May 2 showing the EIT dimming region position at 14:10 UT. The Nancay 236 MHz image at 13:48:21 UT is overplotted in contours. At the time of the EIT image, this radio source had already disappeared. From Pohjolainen *et al.* 2001.

sites of coronal electron acceleration which continues long after the CME has left the low corona (Pick 1986).

### 2.3 Detection of CME-associated structures

EUV waves emanating from sites of active region transients have been recently detected with EIT (Thompson *et al.* 1999). They are closely correlated with CMEs (Biesecker *et al.* 2002) but flares and metric type-II bursts also occur during these events (Klassen *et al.* 2000; Klassen & Aurass 2002). What is the trigger or the nature of these waves is still unclear. In that respect, radio imaging of these phenomena may shed some light. For example, Gopalswamy *et al.* 2000 reported the imaging of a type-II source at 164 MHz coincident with the location of a brow-shaped EIT wave. The thermal radio counterpart of another EIT wave was detected at 17 GHz (White & Thompson 2002). These two observations suggest that there might be two classes of EIT waves. Waves with sharp fronts may be MHD, flare-associated waves while EIT waves with diffused fronts may be associated with CMEs and might trace material pile-up low in the corona.

Bastian *et al.* 2001 carefully analyzed the faint emissions from the 1998 April 20 CME and were able to detect, for the first time, radio loops behind the

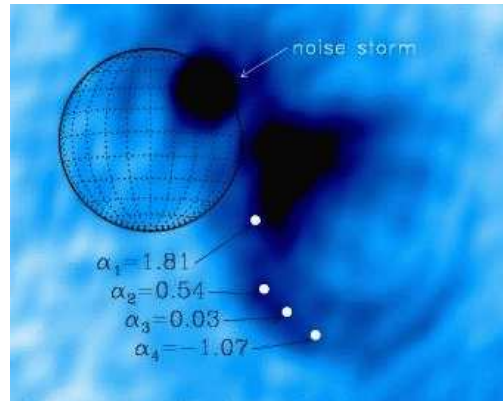


Figure 11.7. Snapshot map of the radio CME loops at 164 MHz. The background disk emission has been removed. A noise storm is present at the northwest. The spectral indices at a few locations are also shown. From Bastian *et al.* 2001

CME front (Figure 11.7). The emission was found to be non-thermal gyrosynchrotron from 0.5–5 MeV electrons. The detection of the loops in several of the NRH frequencies enabled the calculation of spectral indices along the loops. By fitting these lines of sight, Bastian *et al.* 2001 derived additional physical parameters (e.g., density of thermal electrons, magnetic field). Observations of this type will open the possibility of more accurate diagnostics (e.g., thermal density, filling factors) for CME structures.

Gopalswamy, Hanaoka & Lemen 1998 reports the detection of a flare-associated plasmoid at 17 GHz. This is likely the highest frequency type-IVm burst detected and gives information on non-thermal electrons in the cores of CMEs. Plasmoids were detected at 164 MHz in the wake of large eruptions (Vourlidas *et al.* 1999) and they were suggested as the possible sources of some IP bursts.

## 2.4 Radio Prominence Eruptions

H $\alpha$  prominence eruptions have long been used as proxies to coronal ejections (Morrison 1954). The H $\alpha$  emission depends critically on the temperature of the plasma and therefore provides an incomplete picture of the eruption. Because of their low temperature ( $\sim 8000$  K) and high density ( $\sim 10^{10} - 10^{11}$  cm $^{-3}$ ), prominences are optically thick at most microwave frequencies and can be easily observed even at 17 GHz (Gopalswamy & Hanaoka 1998). During eruption, the prominence heats and expands, resulting in changes in its brightness temperature and optical thickness (Gopalswamy, Hanaoka & Lemen 1998). Because prominences are likely to become the white light CME core (Illing & Hundhausen 1985), their analysis is important. In such a study, Hori 2000

found that the appearance or not of a CME core depends on the density of the radio prominence. Estimates of the prominence mass and the dynamics of the early eruption can also be derived from radio data (Gopalswamy & Hanaoka 1998; Gopalswamy *et al.* 1999). These mass estimates are of limited value, however, as the amount of material that drains back to the surface is unknown. It is worth noting that the analysis of a filament eruption at 5 GHz is one of the first results to come out from the renovated Siberian Solar Radio Telescope (Uralov *et al.* 2002).

In addition, careful data reduction of NRH observations of filament eruptions at 410 MHz (Marqué *et al.* 2002) demonstrated that both the filament and the precursor to the white light CME cavity can be imaged and their development followed with high cadence. These results demonstrate that two elements (cavity and core) of the three-part structure of the nominal CME (front, cavity and core) can be imaged and analyzed from radio observations of prominence eruptions. More work is needed in this area to exploit the full potential of these observations.

## 2.5 Type-II emission

Type-II bursts are frequency drifting radio emissions caused by a physical agent propagating outwards in the solar corona (Wild & McCready 1950). Their agent is considered to be an MHD shock (Uchida 1960). They were among the first discoveries in radioastronomy (Payne-Scott, Yabsley & Bolton 1947) and have been used as a proxy for solar eruptive phenomena ever since, so a very large literature on type-II emission has developed. Gopalswamy 2000 gives a recent in-depth review of this phenomenon. Here we focus on a couple of issues that relate to the type-II/CME analyses. The correlation between type-II bursts and CMEs remains controversial (Gopalswamy *et al.* 1998*b*; Cliver, Webb & Howard 1999). The main reason is that the relative timing of flares, CMEs and type-II bursts cannot be established sufficiently accurately with the current instrumentation, although some efforts have been made (Leblanc *et al.* 2001). The connection between metric and decimetric type-IIs is also unclear. Leblanc *et al.* 2001 argue that type-IIs can be followed from the Sun to the Earth, while Reiner *et al.* 2001 concludes that two independent shocks are needed to explain the observations. The rarity of type-II imaging during CME events (Gary *et al.* (1984)) contributes to the confusion. Most type-IIs appear at frequencies below those that can currently be imaged routinely (164 MHz at NRH). GMRT is in principle capable of observing at 50 MHz but this feature has not been implemented yet. Besides, GMRT is not a solar-dedicated instrument. This area of research needs to be addressed by future instrumentation because type-II bursts can tell us a lot about shocks and their evolution in IP space and could have important implications for space weather studies.

## 2.6 CME radio precursors

Radio observations of the corona can contribute also to the search for CME precursors, which are needed for operational applications. In a recent work Aurass *et al.* 1999 proposed that faint drifting continua might indicate the opening of the coronal structures just before the eruption takes place. Their conclusion is based on only two events, however. More extensive searches for these faint radio signatures are needed before drawing firmer conclusions. Another possible candidate are noise storms (Elgaroy 1977). This radio emission is associated with coronal changes such as mass addition (Kerdran *et al.* 1983), large scale magnetic field restructuring (Habbal *et al.* 1996) and filament disappearance (Lantos *et al.* 1981; Pick *et al.* 1995; Marqué *et al.* 2001). A recent statistical study (Ramesh & Sundaram 2001) on the temporal correlation between noise storms and CMEs has been inconclusive. Another study, Chertok *et al.* 2001, found that sharp decreases of the noise storm radio emission are correlated with the passage of the CME material. It seems that the two phenomena are somehow interrelated but the details of the relationship (physical, temporal and/or spatial) are still unclear.

## 2.7 Overview

The above review hopefully demonstrates the importance of radio observations to many aspects of the CME phenomenon. Their contributions to our still incomplete, understanding of these events can be summarized into a “typical radio CME”. In this respect, therefore, a typical radio CME:

- takes less than 15 minutes to fully develop in the low corona. By “fully develop”, I mean that the CME and its associated disturbances have spread throughout the solar disk.
- During its evolution, multiple loop systems, at distant locations (active regions), become active and participate in the eruption by contributing to the ejecta. Determining the participating systems can also help in selecting viable CME initiation models (Maia *et al.* 2003).
- The ejections continue for tens of minutes, even after the main CME body (as witnessed by the white light observations) has left the corona. This suggests that particle acceleration also continues in the wake of the CME. The delayed ejections can drive shocks, interact with the earlier ejecta and therefore may be important for understanding in-situ observations and space weather.
- Structures that are commonly used as CME proxies (EIT waves) might not be related to CMEs at all but rather to co-temporal flares.

- Both the cavity and the core of a typical 3-part white light CME can be imaged in a radio CME. The much higher cadence, provided by the radio instruments, allow us to follow the early phases of the eruption in detail. The core of a typical CME is part of an ejected prominence and its mass can be estimated from the radio measurements.
- Well-defined loops can still be seen within the CME at large heights (2–3  $R_{\odot}$ ), and contain energetic particles with energies of the order of 1 MeV interacting with  $\sim 1$  G magnetic fields.

### 3. FASR Connection

The solar activity that mostly affects the interplanetary space and consequently the Earth environment is the CME activity as seen through white light observations. As such, white light coronagraphs carry the bulk of the research effort. However, their principle of operation—occluding the solar disk—is also their major shortcoming. The birth, drivers and initial stages of the ejection event cannot be monitored. The best solution, so far, has been accomplished by the LASCO and EIT instruments observing the ejections from the disk to the outer corona. These two instrument suites, working as a complement, have contributed to coronal physics and space weather studies to such a degree that all of the future solar NASA missions (*STEREO*, *SDO*) require an EUV disk imager/whitelight coronagraph suite. It does not mean, however, that this approach does not also have its shortcomings. Space-based observations are restricted by the available telemetry and therefore the observing cadence and data gathering ability are compromised compared to ground-based instruments. EUV telescopes are only able to image the solar disk over a narrow temperature range and might miss CME activity outside of their bandpass. Coronagraphs able to image the corona below about  $1.5 R_{\odot}$  are very complex and therefore expensive to build. For these reasons, it is difficult to identify and follow CME structures from the EUV to the white light fields of view. This ambiguity plagues the CME modeling efforts, for example.

Radio instruments have their own problems when they are used for CME observations. But they also have the potential to contribute to the areas where space-based instruments cannot.

#### 3.1 Advantages of Radio Observations

From the work discussed in the previous section, one can derive several key areas radio observations offer (or have the potential to offer) significant insights in the problem of CMEs.

- Accurate timing of CME initiation.
- Positional info on type-II /shock.

- Identify the sites of electron acceleration.
- Follow event from cradle to Earth.
- When emission mechanism is thermal or gyrosynchrotron, derivation of physical parameters (e.g., electron density, magnetic field, energy distribution) inside the CME is possible.

### 3.2 Disadvantages of Current Radio Observations

- Incomplete spectral coverage.
- It is difficult to combine different spectrometer data due to their varying sensitivity, calibration, frequency coverage, RFI environment, etc.
- Imaging unavailable in many frequencies.
- Higher sensitivity is needed for both imaging and spectral observations.
- Physical interpretation of important radio emissions, such as type-IIs, is still incomplete. It reduces the scientific return of these radio observations (for modeling purposes, for example).

### 3.3 Instrument Requirements

Clearly, we need an instrument capable of both broadband spectroscopy and imaging. The requirements that such an instrument must satisfy are:

- (a) It should be able to image the bulk of the ejected material for both limb and earth-directed CMEs. This requires the detection of thermal free-free emission over the background disk emission and the much stronger non-thermal emissions that accompany CMEs. Because the brightness of the thermal CME is frequency-dependent, there is a range of frequencies that would be optimum for detection (Figure 11.2). This range lies between about 0.2–2 GHz where a dynamic range of  $\sim 10$  is sufficient to detect CMEs over the disk background. Non-thermal emission can easily reach brightness temperatures of  $10^9$  K (e.g. plasma emission). Since the thermal CME emission is expected to be about  $10^4 - 10^5$  K, a dynamic range of at least  $10^4$  is needed in this case.
- (b) The thermal emission should be imaged at a cadence sufficient to follow the CME evolution on the disk and low corona and to provide meaningful speed measurements. Given that a typical CME takes about 15 min to develop, a radio map of the full disk every minute with the dynamic range stated in (a) should be sufficient.

- (c) We already know from the Nançay observations (Maia *et al.* 1999; Pohjola *et al.* 2001) that non-thermal sources exhibit significant evolution over 1 s timescales (loop illuminations, short-lived bursts, etc.). Thus, snapshot images every few seconds would allow us a better understanding of the high energy processes involved in the CME, pinpointing shock origins, the relation between flare and CME evolution, etc.
- (d) The instrument should have a large field of view to image CMEs beyond the disk. This will provide the connection to the white light coronagraph field of view, which generally starts at  $\sim 2R_{\odot}$ , and so will allow the study of the acceleration profile and the dynamics of the events and help elucidate the large scale implications of CMEs, such as effects on streamers.
- (e) Finally, the instrument must be able to observe in as many frequencies as possible and to switch among them in a rapid fashion. This way, terrestrial interference and confusing (bright) solar emissions can be avoided and the observations can be tailored to individual events. Another advantage of multi-frequency capability is the use of frequency synthesis techniques (Conway, Cornwell & Wilkenson 1990) to improve the quality of the maps with a minimum impact on hardware.

An instrument that can satisfy all these requirements is an interferometric array designed for Fourier synthesis imaging (e.g., like the VLA). Such an instrument has been proposed under the name Frequency Agile Solar Radiotelescope (FASR) (Bastian, Gary & White 1999) and has been received very well by the community. It is now the number one recommendation of the Solar and Space Physics survey Committee. The instrument concept and implementation is presented in this volume (Bastian, Chapter 3).

Although the design details (e.g., number of antennas, array shape, etc) have not been finalized yet, the viability of CME detection by such an array has been assessed by Bastian & Gary 1997. They simulated an off-limb CME ( $\sim 10^{16}$  g of material) and used three different methods to detect it: (i) direct snapshot imaging at a single frequency, (ii) vector subtraction of CME visibilities between two snapshots (the radio equivalent of running difference) and (iii) vector subtraction for a temporally redundant array. In other words, an array that has identical  $uv$  coverage for images taken at a certain cadence,  $\Delta t$  where  $\Delta t$  is of the order of several minutes. It turns out that the last technique achieves the best results (Figure 11.8) based on a 73-element array (split into two subarrays of 37 elements each).

Detection of CMEs against the solar disk is one of the more important tasks for FASR. Based on the observations reviewed in §2 and the simulations above, it appears that an array with a large number of elements, frequency agility, large

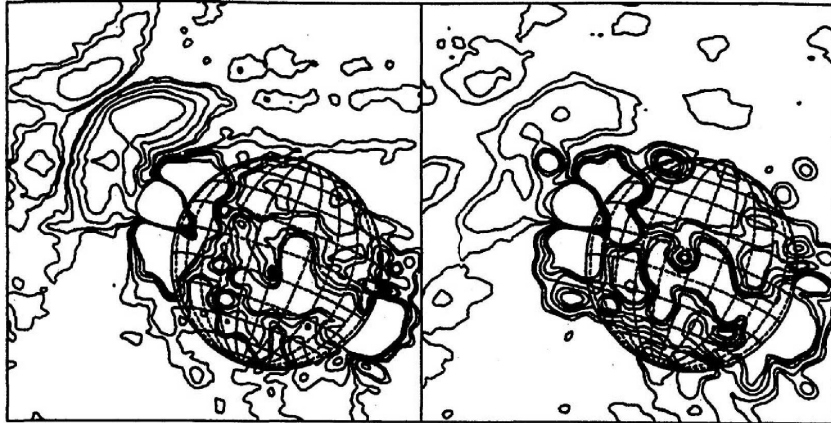


Figure 11.8. Simulation of CME detection by a temporally redundant array. Left panel: Results from a 73-element array. Right panel: Results from a 37-element array. The contour levels are 1, 2, 5, 10, 20  $\times 10^5$  K. From Bastian & Gary 1997.

bandwidth and fast cadence will be able to detect disk CMEs. One should not underestimate source motion as an important factor in pattern recognition. An observer can distinguish a traveling feature in the presence of noise, even if the feature is not readily detectable in a single frame. The detection of EIT waves is a superb example of the power of this technique. These waves are usually undetectable in normal EIT images and barely visible in single difference frames. In a movie sequence of difference, though, the wave becomes visible and can be analyzed. The discussion so far concerned mainly the thermal radio emission. On-disk non-thermal sources (e.g. gyrosynchrotron) are expected to be easily detectable even with a relatively small number of non-thermal electrons entrained in the CME (Figure 8 in Bastian & Gary 1997).

In conclusion, the power of radio observations lies in their flexibility and access to the many facets of coronal mass ejections (bulk material, shocks, waves, prominence eruptions). The ability to obtain information on the physical parameters of the CME and the processes that initiate these phenomena has been demonstrated above. The next step is to design, build and operate FASR, a radio instrument that will exploit this potential.

### Acknowledgments

I wish to thank N. Gopalswamy and S. Plunkett for useful discussions. A.V. research is supported by various NASA and ONR grants. SOHO is an international collaboration between NASA and ESA and is part of the International Solar Terrestrial Physics Program. LASCO was constructed by a consortium of institutions: the Naval Research Laboratory (Washington, DC, USA), the University of Birmingham (Birmingham, UK), the Max-Planck-Institut für

Aeronomie (Katlenburg-Lindau, Germany) and the Laboratoire d'Astronomie Spatiale (Marseille, France).

## References

- Aurass, H., Vourlidas, A., Andrews, M. D., Thompson, B. J., Howard, R. H. & Mann, G. 1999, *ApJ*, 511, 451
- Bastian, T. S. & Gary, D. E. 1997, *JGR*, 102, 14031
- Bastian, T. S., Benz, A. O. & Gary, D. E. 1998, *ARAA*, 36, 131
- Bastian, T. S., Gary, D. E. & White, S. M. 1999, Report to the Astronomy and Astrophysics Survey Committee
- Bastian, T. S., Pick, M., Kerdraon, A., Maia, D. & Vourlidas, A. 2001, *ApJ*, 558, L65
- Bastian, T. S., Chapter 3, this volume
- Biesecker, D. A., Myers, D. C., Thompson, B. J., Hammer, D. M. & Vourlidas, A. 2002, *ApJ*, 569, 1009
- Boichot, A. 1957, *Compt. Rend. Acad. Sci.*, 244, 1326
- Bougeret, J.-L., *et al.* 1995, *Space Sci. Rev.*, 71, 231
- Brueckner, 1995, *Solar Phys*, 163, 357
- Cane, H. V. 1984, *A&A*, 140, 205
- Cane, H. V., Richardson, I. G. & St Cyr, O. C. 2000, *Geophys. Res. Lett.*, 27, 3591
- Chertok, I. M., Kahler, S., Aurass, H. & Gnezdilov, A. A. 2001, *Solar Phys*, 202, 337
- Classen, A. T. & Aurass, H. 2002, *A&A*, 384, 1098
- Cliver, Edward W., Webb, David F., Howard, R. A. 1999, *Solar Phys*, 187, 89
- Conway, J. E., Cornwell, T. J. & Wilkenson, P. N. 1990, *MNRAS*, 246, 490
- Crooker, N., Joselyn, J. A. & Feynman, J. (eds), 1997, *Coronal Mass Ejections*, AGU Geophys. Mon. 99, (AGU: Washington, DC)
- Dulk, G. A. 1985, *ARAA*, 23, 169
- Dulk, G. A., Leblanc, Y., Bastian, T. S., Bougeret, J.-L. 2000, *JGR*, 105, 27343
- Domingo, V., Fleck, B. & Poland, A. I. 1995, *Solar Phys*, 162, 1
- Elgaroy, O. 1977, *Solar Noise Storms*, (Oxford: Pergammon Press)
- Gary, D. E., Dulk, G. A., House, L., Illing, R., Sawyer, C., Wagner, W. J., McLean, D. J. & Hildner, E. 1984, *A&A*, 134, 222
- Gary, D. E. *et al.* 1998, *BAAS*, SPD meeting 30, SH-32A-11
- Gary, D. E. & Hurford, G. J., Chapter 4, this volume.
- Gelfreikh, G. B., Chapter 6, this volume.
- Gopalswamy, N. & Kundu, M. R. 1992, *ApJ*, 390, L37
- Gopalswamy, N. *et al.* 1998a, *GRL*, 25, 2485
- Gopalswamy, N., Kaiser, M. L., Lepping, R. P., Kahler, S. W., Ogilvie, K., Berdichevsky, D., Kondo, T., Isobe, T., Akioka, M. 1998b, *JGR*, 103, 307

- Gopalswamy, N. & Hanaoka, Y. 1998, ApJ, 498, L179
- Gopalswamy, N., Hanaoka, Y. & Lemen, J. R. 1998, in *New Perspectives in Solar Prominences*, IAU Coll. 167, eds D.F. Webb, B. Schmieder & D.M. Rust (San Francisco: ASP)
- Gopalswamy, N. 1999, in *Solar Physics with Radio Observations*, Proc. of the Nobeyama Symp. eds. Bastian, T. S., Gopalswamy, N. & Shibasaki, K., p. 141
- Gopalswamy, N., Kaiser, M. L., Sato, J., Pick, M. 2000, in *High Energy Solar Physics: Anticipating HESSI*, ASP Conf. Ser. 206, eds. R. Ramaty & N. Mandshavidze, 351
- Gopalswamy, N. 2000, in *Radio Astronomy at Long Wavelengths*, AGU Geophys. Mon. 119, eds. R.G. Stone, K.W. Weiler, M.L. Goldstein & J.-L. Bougeret (Washington, DC: AGU), p. 123
- Gopalswamy, N., Yashiro, S., Kaiser, M. L., Howard, R. A., Bougeret, J.-L. 2001, ApJ, 548, L91
- Gold, T. 1955, in *Gas Dynamics of Cosmic Clouds*, IAU, 2, (N.Holland Publ. C: Amsterdam), p.238
- Gosling, J. T., Hildner, E., MacQueen, R. M., Munro, R. H., Poland, A. I., Ross, C. L. 1974, JGR, 79, 4581
- Habbal, S. R., Mossman, A., Gonzalez, R., Esser, R. 1996, JGR, 101, 19943
- Hori, K. 2000, ApJ, 543, 1011
- Howard, R.A. *et al.* 1975, World Data Center Report UAG, 48A
- Howard, R. A., Michels, D. J., Sheeley, N. R., Jr., Koomen, M. J. 1982, ApJ, 263, L101
- Howard, R. A., Sheeley, N. R., Jr., Michels, D. J., Koomen, M. J. 1985, JGR, 90, 8173
- HHundhausen, A. J., Sawyer, C. B., House, L., Illing, R. M. E., Wagner, W. J. 1984, JGR, 89, 2639
- Hundhausen A. J., Burkepile, J.T. & StCyr, O. C. 1994, JGR, 90, 6543
- Hundhausen, A. J., 1999, in *The Many Faces of the Sun*, eds. K.T. Strong, J.L.R. Saba, B.M. Haisch & J.T. Schmelz (New York: Springer), p.143
- Illing, R. M. E. & Hundhausen, A. J. 1985, JGR, 90, 275
- Kahler, S. W., Cliver, E. W., Cane, H. V., McGuire, R. E., Stone, R. G., Sheeley, N. R., Jr. 1986, ApJ, 302, 504
- Kathiravan, C., Ramesh, R. & Subramanian, K. R. 2002, ApJ, 567, L93
- Kerdraon, A. & Delouis, J. M. 1997, in *Coronal Physics from Radio and Space Observations*, ed. G. Trottet (Berlin: Springer) 192
- Kerdraon, A., Pick, M., Trottet, G., Sawyer, C., Illing, R., Wagner, W., House, L. 1983, ApJ, 265, L21
- Klassen, A., Aurass, H., Mann, G., Thompson, B. J. 2000, A&ASupp., 141, 357

- Landos, P. 1980, in *Radio Physics of the Sun*, Kundu, M.R. & Gergely, T.E. (eds), (Norwell, MA: D. Reidel), 41
- Lantos, P., Kerdraon, A., Rapley, G. G., Bentley, R. D. 1981, *A&A*, 101, 33
- Leblanc, Y. *et al.* 2000, *JGR*, 105, 18225
- Leblanc, Y., Dulk, G. A., Vourlidas, A., Bougeret, J.-L. 2001, *JGR*, 106, 25301
- Low, B. C. 2001, *JGR*, 106, 25141
- MacQueen, R. M., Csoeke-Poeckh, A., Hildner, E., House, L., Reynolds, R., Stanger, A., Tepoel, H., Wagner, W. 1980, *Solar Phys*, 65, 91
- Maia, D. *et al.* 1998, *Solar Phys*, 181, 121
- Maia, D., Vourlidas, A., Pick, M., Howard, R., Schwenn, R. & Magalhães, A. 1999, *JGR*, 104, 12507
- Maia, D., Pick, M., Vourlidas, A. & Howard, R. 2000, *ApJ*, 528, L49
- Maia, D., Pick, M., Hawkins, S. E., Fomichev, V. V. & Jiřička, K. 2001, *Solar Phys*, 204, 197
- Maia, D., Aulanier, G., Wang, S. J., Pick, M., Malherbe, J.-M. & Delaboudinière, J.-P. 2003, *A&A*, 405, 313
- Manoharan, P. K., Tokumaru, M., Pick, M., Subramanian, P., Ipavich, F. M., Schenk, K., Kaiser, M. L., Lepping, R. P., Vourlidas, A. 2001, *ApJ*, 559, 1180
- Marqué, C., Lantos, P., Klein, K.-L. & Delouis, J. M. 2001, *A&A*, 374, 316
- Marqué, C., Lantos, P. & Delaboudinière, J. P. 2002, *A&A*, 387, 317
- Michels, D. J., Howard, R. A., Koomen, M. J., Sheeley, N. R., Jr. 1980, in *Radio Physics of the Sun*, IAU 86, eds Kundu, M.R. & Gergely, T., (Hingman: D. Reidel)p. 439
- Morrison, P. 1954, *Phys. Rev.*, 95, 440
- Nakajima, H. *et al.* 1994, *Proc. IEEE*, 82, 705
- Payne-Scott, R., Yabsley, D. E. & Bolton, J. G. 1947, *Nature*, 160, 256
- Pick, M. 1986, *Solar Phys*, 104, 19
- Pick, M., Buttighoffer, A., Kerdraon, A., Armstrong, T. P., Roelof, E. C., Hoang, S., Lanzerotti, L. J., Simnett, G. M., Lemen, J. 1995, *Sp. Sc. Rev.*, 72, 315
- Pick, M. *et al.* 1998, *Solar Phys*, 181, 455
- Plunkett, S. P., Vourlidas, A., Simberová, S., Karlický, M., Kotrc, P., Heinzel, P., Kupryakov, Yu. A., Guo, W. P., Wu, S. T. 2001, *Solar Phys*, 194, 371
- Pohjolainen, S., Maia, D., Pick, M., Vilmer, N., Khan, J. I., Otruba, W., Warmuth, A., Benz, A., Alissandrakis, C., Thompson, B. J. 2001, *ApJ*, 556, 421
- Ramesh, R., Subramanian, K. R., Sundararajan, M. S., Sastry, Ch. V. 1998, *Solar Phys*, 181, 439
- Ramesh, R. & Shanmugha Sundaram, G. A. 2001, *Solar Phys*, 202, 355
- Rames, D. V. 1999, *Space Sci. Rev*, 90, 413
- Reiner, M. J., Kaiser, M. L., Gopalswamy, N., Aurass, H., Mann, G., Vourlidas, A., Maksimovic, M. 2001, *JGR*, 106, 25279
- Sheeley, N. R., Jr., Howard, R. A., Michels, D. J., Koomen, M. J., Schwenn, R., Muehlhaeuser, K. H., Rosenbauer, H. 1985, *JGR*, 90, 163

- Sheridan, K. V., Jackson, B. V., McLearn, D. J. & Dulk, G. A. 1978, *Proc. Astr. Soc. Aus.*, 3, 249
- St. Cyr, O. C., Burkepile, J. T., Hundhausen, A. J. & Lecinski, A. R. 1999, *JGR*, 104, 12493
- Stewart, R. T., 1985, in *Solar Radiophysics*, McLean, D.J & Labrum, N.R. eds, (London:Cam. Univ. Press), p. 361
- Thompson, B. J., Gurman, J. B., Neupert, W. M., Newmark, J. S., Delaboudinière, J.-P., St. Cyr, O. C., Stezelberger, S., Dere, K. P., Howard, R. A., Michels, D. J. 1999, *ApJ*, 517, L151
- Tousey, R. 1973, in *Space Research XIII*, ed. M.J. Rycroft & S.K. Runcorn (Berlin:Academie-Verlag), p.173
- Uchida, Y. 1960, *PASJ*, 12, 376
- Uralov, A. M., Lesovoi, S. V., Zandanov, V. G. & Grechnev, V. V. 2002, *Solar Phys*, 208, 69
- Vourlidas, A., Maia, D., Pick, M., Howard, R. A. 1999, in *Proc. of the 9th Eur. Mtg on Solar Physics*, ed. R. Willson, ESA SP-448, 1003
- Vourlidas, A., Howard, R. A., Morrill, J. S., Munz, S. 2002, in *Solar-Terrestrial Magnetic Activity & Space Environment*, COSPAR Coll. Ser. 14, Wang, H.N. & Xu, R.K. (eds), (London: Pergammon), p. 201
- Wang, Z., Schmahl, E.J. & Kundu, M. R. 1987, *Solar Phys*, 111, 419
- Wagner, W. J., Hildner, E., House, L. L., Sawyer, C., Sheridan, K. V. & Dulk, G. A. 1981, *ApJ*, 244, L123
- Webb, D. F., Cliver, E. W., Crooker, N. U., St. Cyr, O. C., Thompson, B. J. 2000, *JGR*, 105, 7491
- Webb, D. F. *et al.* 2001, in *Space Weather*, AGU Geophys. Mon. 125, Song, P., Singer, H.J. & Siscoe, G.L. (eds), 123
- White, S. M. & Thompson, B. J. 2002, *AAS Meeting*, 200.2904
- Wild, J. P. & McCready, L. L. 1950, *Aus. J. Sci. Res.*, A3, 387
- Zirin, H., Baumert, B. M. & Hurford, G. J., 1991, *ApJ*, 370, 779